Title: Clean synthesis of alkyl levulinates from levulinic acid over one pot synthesized WO_3-SBA-16 catalyst

Author: Enumula Siva Sankar Gurram Venkata Ramesh Babu Chada Raji Reddy Burri David Raju Kamaraju Seetha Rama Rao

PII: S1381-1169(16)30455-1
DOI: http://dx.doi.org/doi:10.1016/j.molcata.2016.10.032
Reference: MOLCAA 10094

To appear in: *Journal of Molecular Catalysis A: Chemical*

Received date: 23-7-2016
Revised date: 29-9-2016
Accepted date: 29-10-2016

Please cite this article as: Enumula Siva Sankar, Gurram Venkata Ramesh Babu, Chada Raji Reddy, Burri David Raju, Kamaraju Seetha Rama Rao, Clean synthesis of alkyl levulinates from levulinic acid over one pot synthesized WO3-SBA-16 catalyst, Journal of Molecular Catalysis A: Chemical http://dx.doi.org/10.1016/j.molcata.2016.10.032

Clean synthesis of alkyl levulinates from levulinic acid over one pot synthesized WO_3-SBA-16 catalyst

Enumula Siva Sankar, Gurram Venkata Ramesh Babu , Chada Raji Reddy, Burri David Raju, Kamaraju Seetha Rama Rao *

Inorganic and Physical Chemistry Division, CSIR-Indian Institute of Chemical Technology, Hyderabad, India-5000071. E-mail: ksramarao@iict.res.in & ksramarao.iict@gov.in

Fax: +91-40-27160921; Tel: +91-40-27193163

Graphical abstract

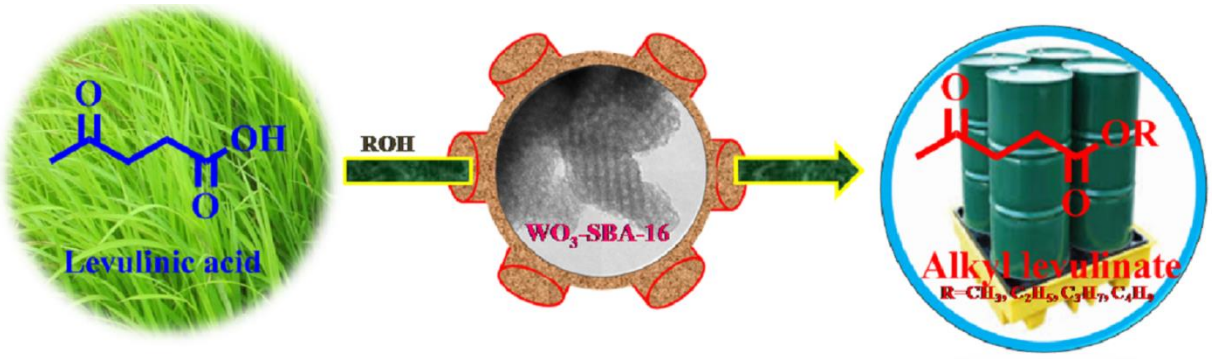

Esterification of Levulinic acid with alcohols over one pot synthesized WO_3-SBA-16 catalyst in continuous process at atmospheric pressure.

Highlights

- Retainment of mesoporous nature after incorporation of WO_3 during the preparation of SBA-16
- Doping WO_3 into SBA-16 increases the acidity
- Among the catalysts, 3 weight % WO_3-SBA-16 is optimum for levulinic acid esterification
- 3 weight% WO_3-SBA-16 catalyst exhibits steady activity during time on stream operation for 10 cycles

Abstract:

The present work highlights the application of solid acid catalyst to produce alkyl levulinate from levulinic acid in continuous mode under vapor phase conditions. In this context, tungsten oxide incorporated SBA-16 catalysts were prepared by one pot direct synthesis method and evaluated for the titled reaction. Under optimized reaction conditions, 3 weight % WO_3-SBA-16 catalyst delivered complete conversion of levulinic acid with 95% selectivity towards ethyl levulinate. The synthesized catalysts were characterized to know the physico-chemical features by various techniques, namely, X-ray diffraction, N_2 physisorption, temperature programmed reduction of hydrogen (H_2-TPR), temperature programmed desorption of ammonia (NH_3-TPD), DR-UV-visible spectroscopy, Fourier transform infrared (FTIR) spectroscopy, transmission electron microscopy (TEM) and scanning electron microscopy (SEM). The characterization results suggest that, the superior catalytic activity can be ascribed due to the enhanced acidity of SBA-16 obtained through incorporation of tungsten oxide and easy of accessibility for the dispersed active sites through uniform pore channels. The constant catalytic activity in 10 h time

on study shows the sturdiness of the catalyst and the spent catalyst can be regenerated several times. Moreover, various alkyl levulinates (methyl, n-propyl, and n-butyl) were synthesized with more than 90% selectivity over this catalyst.

Key words: Levulinic acid, Esterification, Tungsten oxide, SBA-16

1. Introduction

At present the World's energy demand is alarming to cater the needs of upcoming generations, because the petro industry is producing fuels and chemicals from the fossil resources in an uninterrupted way. In this scenario, the production of bio based fuels has attracted much attention to overcome the reliance on depleting fossil resources [1-2]. However, the production of bio-fuels from starch and edible oil was associated with complications such as their feedstock availability would be competitive with food supply and undesirable effects on land requirements creating food versus fuel problem. Now the present ongoing research activities have been switched over to the production of bio-fuels from renewable, abundant, non-food lignocellulosic biomass [3-4]. The lignocellulosic biomass (composed of 40–50% cellulose, 16–33% hemicelluloses and 15–30% lignin) identified as source of carbon raw materials for the synthesis of variety of compounds [5]. The carbohydrate fractions of lignocellulosic biomass are hemicelluloses and cellulose which can be converted into fuels, fuel additives and chemicals in multiple steps [6-8]. In those conversions, esterification of levulinic acid is a promising route to synthesize alkyl levulinates such as methyl, ethyl, propyl, and n-butyl levulinates. In this particular conversion, the reactant, levulinic acid (LA) was identified as one of the top most platform chemical that can be obtained from lignocellulosic biomass and the products alkyl levulinates were found to be having potential applications in transportation fuel sector,

production of fine chemicals, as plasticizers, as precursors in flavoring and fragrance industries [9-11]. Among these alkyl levulinates, ethyl levulinate (EL) has been enticed due to its miscibility with gasoline and diesel fuels with attributing modifications such as high lubricity, stable flash point, decrease in sulfur content, flow properties under cold conditions. EL can be added up to 5 wt% as an additive in the diesel fuel directly. Recent studies suggest that EL can be used as blending agent for biodiesel. Upon the addition of 20 vol % EL to bio-diesel derived from cottonseed oils, the fuel properties of the bio-diesel were improved [12-13]. Owing to versatile applications of EL, its synthesis would be fascinating. Conventionally, the esterification of LA with alcohols was carried out by using mineral acids creating environmental issues, recyclability problems, and need of neutralization after the reaction, made these processes as insignificant. Several contemporary works have been reported to develop greener approaches for the production of EL over solid acid catalysts such as supported or modified hetero poly acids, sulfated metal oxides, and zeolites with inspiring activities [14-18]. However, most of these reactions are employed in batch conditions. Synthesis of EL in continuous process is advantageous with regard to avoiding neutralization after the reaction, ease of catalyst separation, and reaction continuation for longer hours. Tungsten oxide, based catalysts have been reported in numerous acid catalyzed reactions like isomerization of alkenes, hydrodesulphurization and hydro cracking of heavy fractions in the petroleum chemistry [19-20]. Mesoporous silica (SBA-16) having 3D cubic arrangement with cage like structure possessing unique characteristics like thermally stable pore walls, high surface areas and pore volumes to disperse the active species, has been regarded as a suitable support for various applications including catalytic conversions of biomass derived platform chemicals to value added products [21-24]. The doped mesoporous silica, SBA-16 materials are emerging as the desired

physicochemical properties of the catalysts can be achieved in one pot direct synthesis thereby decreasing the multistep process in the catalysts synthesis [25-26]. In our previous work aiming for the synthesis of alkyl levulinates over ZrO_2/SBA-15 catalyst, formation of gamma-valerolactone was observed with alcohols like ethanol, propanol, and butanol. The formation of gamma-valerolactone via catalytic transfer hydrogenation (MPV reduction) decreases the selectivity to alkyl levulinates such as ethyl, propyl, and butyl levulinates [27]. Hence, in order to obtain maximum selectivity to alkyl levulinates development of catalysts which do not promote the catalytic transfer hydrogenation of levulinic acid with alcohols like ethanol, propanol and butanol is necessary. In this scenario an attempt has been made to prepare tungsten oxide incorporated SBA-16 catalysts with various loadings by means of one pot direct synthesis method for the selective synthesis of alkyl levulinates from levulinic acid in a continuous process at atmospheric pressure in a fixed bed reactor.

2. Experimental

2.1. Catalyst preparation

SBA-16 mesoporous silica and tungsten oxide doped SBA-16 materials were prepared according to literature described elsewhere by using Pluronic F127 triblock polymer ($EO_{106}PO_{70}EO_{106}$, called F127, M/s. Sigma Aldrich chemicals, USA) as structure directing agent, tetra ethyl ortho silicate (TEOS, M/s. Sigma-Aldrich chemicals, USA) as silica source, sodium tungstate as tungsten oxide precursor and n-butanol as co-surfactant [26,28]. In a characteristic synthesis 3.5 g of F127 dissolved in 175 mL of 0.4M HCl solution at 45 °C, then 13 mL of n-butanol was added with stirring. After 1 h stirring, 16.7 g of TEOS and requisite amount of sodium tungstate were added to the mixture and the stirring was continued for 20 h. Then it is kept under static hydrothermal treatment at 100 °C for 24 h. It was filtered and dried at 100 °C

for 12 h and then dried solid was calcined at 550 °C for 6 h in air flow. The resultant solid was labeled as XWS where X indicates the weight percentage of tungsten oxide incorporated in SBA-16 and tungsten oxide alone was prepared in a conventional precipitation method. For comparison purpose 3 wt% WO_3/SBA-16 catalyst was prepared by impregnation method and labeled as 3WS-I.

2.2. Characterization of catalysts

The X-ray diffraction patterns were recorded on an Ultima-IV (M/s. Rigaku Corporation, Japan) operated at 40 kV and 40 mA equipped with nickel-filtered Cu Kα radiation (λ =1.54056 Å). The BET surface areas, pore volume and pore sizes were determined by using the N_2 physisorption-desorption studies (M/s. Quantachrome Instruments, USA, samples were degassed at 150 °C for 2 h) by nitrogen adsorption at liquid N_2 temperature. The UV–Vis spectra were recorded on a UV-2000, (M/s Shimadzu, Japan) spectrophotometer with $BaSO_4$ as a reference material. The temperature programmed desorption of ammonia (NH_3-TPD) was performed as follows, Approximately, 50 mg of catalyst sample was placed in a quartz reactor and pretreated in a flow of helium (30 mL min^{-1}) at 400 °C for 2 h. Subsequently, the catalyst sample was saturated with 10% NH_3/He (30 mL min^{-1}) at 80 °C for 30 min. then the helium was allowed to flow for 30 min at 100 °C for complete removal of physisorbed ammonia. Helium flow was continued while increasing the temperature to 500 °C at a ramp of 10 °C min^{-1} and the desorbed NH_3 was monitored with on-line connected thermal conductivity detector (TCD) equipped GC. Temperature programmed reduction of hydrogen (H_2-TPR) was performed on a homemade TPR system. Typically, About 50 mg of the catalyst was placed in a quartz reactor and pre-treated in Helium flow (30 ml min^{-1}) at 300 °C for 1 h. Later, the catalyst was treated with 5% H_2–Ar mixture gas (30 ml min^{-1}) while increasing the temperature up to 1000 °C

with a temperature ramp of 10 °C min^{-1} and it was monitored using a thermal conductivity detector. The FTIR spectra were recorded on a spectrum GX spectrometer (M/s. Perkin-Elmer, Germany) in the scan range of 1400–400 cm^{-1}. The pyridine adsorption studies were carried out in the diffuse reflectance infra red Fourier transform (DRIFT) mode. In the typical experiment the catalyst was degassed under vacuum at 200 °C for 3 h followed by suspending dry pyridine. Then, the excess pyridine was removed by heating the sample at 120 °C for1 h. After cooling the sample to room temperature, FT-IR spectra of the pyridine-adsorbed samples were recorded. SEM images of the catalysts were recorded on a scanning electron microscope (M/s. JEOL, Switzerland) and TEM images were obtained on a JEM 2000EXII apparatus (M/s. JEOL, Switzerland) respectively. Prior to TEM analysis, the catalyst sample was ultrasonicated in ethanol and a drop was placed onto the carbon coated copper grid, the solvent was then dried in an air oven at 80 °C for 6 h.

2.3. Catalytic activity

The catalytic activity tests were conducted in fixed bed down flow reactor (14 mm id and 300 mm length) at atmospheric conditions. In a typical experiment about 0.5 g of the catalyst was mixed with same amount of quartz particles and sandwiched between two plugs at the centre of the reactor. Before the catalytic run, the catalyst was preheated in N_2 flow (30 mL min^{-1}) at 250 °C for 1 h. The liquid feed with required molar ratio of levulinic acid and alcohol was fed at a flow rate of 1 ml/h using syringe feed pump (M/s. B. Braun, Germany). The product mixture collected from an ice cooled trap was analyzed by FID equipped GC-17A (M/s. Shimadzu Instruments, Japan) with EB–5 capillary column (30 m x 0.53 mm x 5.0 µm) and confirmed by GC-MS, QP-2010 (M/s. Shimadzu Instruments, Japan) with EB–5 MS capillary column (30 m x 0.25 mm x 0.25 µm).

3. Results and discussion

3.1. Catalyst characterization

The powder X-ray diffraction patterns of the SBA-16 and WO_3-SBA-16 samples were shown in Figure 1. From low angle XRD patterns, it can be observed that SBA-16, and tungsten oxide incorporated SBA-16 samples have retained their 3D pore arrangement, by exhibiting three diffraction peaks at 2θ values around 0.8°, 1.0° and 1.1° corresponding to the (110), (200) and (211) planes respectively, of regular mesoporous 3D cubic pore (Im3m) structure [28,29]. The $d_{(110)}$ and unit cell parameter (a_o) values presented in Table 1 indicates the evenness of mesoporous 3D cubic structure even after tungsten oxide incorporation into SBA-16. However, there is a shift of (110) reflection to lower angles in the low angle XRD patterns of the tungsten oxide incorporation which causes increase in the unit cell parameters of the WO_3-SBA-16 samples. It can be attributed to the incorporation of tungsten having higher atomic radius compared to the Si^{+4} frame work of SBA-16. These results suggest the tungsten oxide incorporation into SBA-16 frame work [30, 31, 34]. Wide angle XRD patterns (Figure 1 inset) SBA-16 and WO_3-SBA-16 samples show a broad peak in the 2θ region of 15-30° which is characteristic peak for amorphous silica. No crystalline peaks of WO_3 are found in the tungsten oxide incorporated SBA-16 samples designating the existence of amorphous form or highly dispersed WO_3 species in the SBA-16 [26, 32]. From the EDX analysis, the presence of tungsten can be observed and the respective weight percentages are presented in Table 2.

The N_2 adsorption-desorption isotherms and pore size distributions of the samples were depicted in Figure 2. From the N_2 sorption isotherms, all the samples, i.e., SBA-16 and tungsten oxide incorporated SBA-16 display type IV isotherm with H2-type hysteresis loop representing

the mesoporous materials with cage like pore structure [26, 28, 33]. For all the samples, capillary condensation was observed within the P/P_0 range of ~ 0.5-0.8 which is characteristic feature for the mesoporous materials. This clearly confirms the intactness of mesoporous structure of the SBA-16 even after tungsten oxide incorporation. The shift in inflection point of isotherms towards higher relative pressure in tungsten oxide incorporated SBA-16 samples compared to SBA-16 was observed due to the incorporation of WO_3 on the walls of mesopores of SBA-16 [34]. Increase in pore diameter of the WO_3-SBA-16 samples can be noticed from the NLDFT calculations. The pore size distributions of the samples (Figure.2 inset) exhibit a bimodal pore size distribution with an average pore size of ~ 4-5 nm which is characteristic feature of cage type mesopores. [26, 35]. The textural and structural parameters of the samples are presented in Table 1. The surface area and pore volumes of the tungsten oxide incorporated samples decreases with increase in the amount of tungsten oxide. Even though, a gradual or slight decrease in surface area per gram catalyst exists, surface area per gram support remains more or less same with increase in WO_3 loading which can be attributed to the incorporation of WO_3 in the SBA-16 framework.

SEM and TEM images of the SBA-16 and 3WS samples were depicted in Figure 3. The morphology of the SBA-16 and 3WS samples show agglomerated spheres like morphology typical of reported SBA-16 materials [36, 37]. It can be observed that 3WS sample is also maintaining the sphere like morphology even after tungsten oxide incorporation in SBA-16. TEM images display the well ordered cubic pore structure in the SBA-16 and tungsten oxide incorporation in SBA-16 sample [38, 39]. The pore channel width of the SBA-16 and 3WS are ~ 9.1 nm and ~10.5 nm respectively. The results from the X-ray diffraction, N_2 physisorption and

electron microscopic images suggest the maintenance of 3D mesoporous cubic arrangement in the SBA-16 and tungsten oxide incorporated SBA-16 samples.

Diffuse reflectance UV-visible spectra of WO_3-SBA-16 samples and bulk WO_3 were presented in Figure 4. WO_3-SBA-16 samples show two absorption bands at around 218 nm and 265 nm. The ligand to metal charge transfer in isolated [WO_4] tetrahedral species results the absorption band at 218 nm, indicating the incorporation of tungsten oxide species in the frame work of SBA-16 [30, 40-42]. The absorption band around 265 nm is due to the charge transfer from O^{2-} to W^{6+} in an octahedrally coordinated tungsten oxide species or isolated tungsten species [41-42]. The absorption band at around 377 nm in the bulk WO_3 designates the presence of tungsten oxide crystallites, which is absent in the WO_3-SBA-16 samples, clearly manifesting the absence of crystalline WO_3 in these samples. These results are parallel with the wide angle XRD patterns of the WO_3-SBA-16 samples.

FT-IR spectra of SBA-16 and WO_3-SBA-16 samples were shown in Figure 5. All the samples display characteristic vibration bands at around 468, 806 and 1084 cm^{-1}, representing typical vibration bands for Si-O-Si structural units [43, 44]. The vibration band at 1084 cm^{-1} with a shoulder at 1245 cm^{-1} can be ascribed to asymmetric stretching and the band at 806 cm^{-1} is due to the symmetric stretching modes of Si-O-Si units [43, 44]. The typical vibration band at 968 cm^{-1} is due to the stretching vibration mode of Si-O-W in the tungsten oxide incorporated SBA-16 samples. As well, the vibration band at 959 cm^{-1} in pure SBA-16 can be attributed to the Si-O stretching of Si-OH groups. The introduction of transition metal atoms in the frame work of silica can change the Si-O stretching vibration mode [43]. The slight shift of the vibration band at 959 cm^{-1} towards higher wave number in the tungsten oxide incorporated SBA-16 samples indicates the presence of tungsten in the frame work of SBA-16 silica [45, 46].

The temperature programmed reduction (H_2-TPR) patterns of tungsten oxide incorporated SBA-16 samples were presented in Figure 6. These patterns show that bulk WO_3 possesses three reduction peaks at around 650, 730 and 880 °C. The high temperature reduction peaks indicate the reduction of tungsten oxide species in tetrahedral coordination and the smaller reduction peak at 650 °C is due to the reduction of supported tungsten oxide crystallites [47-49]. The tungsten oxide incorporated SBA-16 samples show slightly higher reduction temperatures than the bulk tungsten oxide. The 5WS sample exhibits two reduction peaks at 750 and 890 °C. The TPR patterns of 1WS and 3WS show a shift in the reduction temperature to ~915 °C representing the high dispersion of tungsten oxide species [47]. The increase in the reduction temperature may be due to the reduction of highly dispersed tetrahedrally coordinated tungsten species or due to the reduction of frame work tungsten oxide species which are interacted with the silica [49, 50, 26].

The temperature programmed desorption of ammonia (NH_3-TPD) profiles of tungsten oxide incorporated SBA-16 samples were presented in Figure 7 and the respective total acidity values are summarized in Table.2. The acidic sites distribution can be categorized depending upon the desorption temperature of ammonia as weak (< 250 °C) moderate (250-400 °C) and strong acidic sites (> 400 °C) [51]. From the NH_3-TPD profile, the SBA-16 doesn't show any appreciable desorption of ammonia. Whereas the tungsten oxide incorporated SBA-16 samples show desorption peak in the temperature region of 140-280 °C representing the presence of more population of weak acidic sites in the samples. It can be observed that, the incorporation of tungsten oxide into the frame work of SBA-16 leads to the development of higher number of weak acidic sites. The total acidity of the samples is increasing with the increase in amount of tungsten oxide incorporation. Whenever high amount of tungsten oxide incorporated in the frame

work the total acidity decreases due to the formation of crystalline tungsten oxide [26, 34, 47]. In the present investigation, the increase in WO_3 loading is clear indication of the presence of WO_3 within the frame work.

The pyridine adsorbed FT-IR analysis was performed to access the type of acidic sites present on the catalyst surface and their respective patterns were presented in Figure 8. The pure SBA-16 sample possess two adsorption bands at 1446 and 1595 cm^{-1} representing the presence of coordinately bonded pyridine to the surface Lewis acidic sites [53, 54]. In addition to these two bands the tungsten oxide incorporated SBA-16 samples exhibit the bands at 1548 and 1630 cm^{-1} showing the presence of Brønsted acidic sites and one more band at 1489 cm^{-1} result due to the combination of Lewis and Brønsted acidic sites on the catalyst surface [47, 53, 54]. It can be observed that, the incorporation of tungsten oxide in the SBA-16 tends to increase the surface Lewis acidic sites as well as surface Brønsted acidic sites thereby increasing the total acidity of the tungsten oxide incorporated SBA-16. It is obvious from the figure that tungsten oxide incorporated SBA-16 samples exhibit a higher number of Lewis acidic sites compared to Brønsted acidic sites.

3.2. Catalytic activity studies

3.2.1. Effect of WO_3 loading

The influence of tungsten oxide loading on the esterification of levulinic acid was studied in order to know the optimum loading of tungsten oxide and the results were presented in Figure 9. The esterfication of LA with ethanol (EtOH) over pristine SBA-16 and WO_3 results lower conversions of LA 39% and 73% with selectivity's to ethyl levulinate (EL) are 74% and 72% respectively. The incorporation tungsten oxide into the frame work of mesoporous SBA-16

shows greater selectivity to EL due to enhanced acidity obtained through the dispersed acidic sites of incorporated tungsten oxide over larger surface areas of SBA-16. The conversions of LA and selectivity to EL increases with increasing amount of tungsten oxide. The conversions of LA over 1WS and 3WS are 92% and 100% with selectivity's to EL are 78% and 95% respectively. Further increase in the amount of tungsten oxide (5WS) results no considerable change in the selectivity to EL. The acidity of 3WS catalyst is enough to catalyze the esterification of LA to yield EL with maximum selectivity. The high catalytic performance of these catalysts signifies the easy accessibility of the active acidic sites in the mesostructured tungsten oxide incorporated SBA-16 catalysts. The formation of levulinate ester and angelica lactones may proceed through the probable mechanism as shown in Scheme 1 and 2 respectively. As evident from the pyridine adsorbed FT-IR analysis the tungsten oxide incorporated SBA-16 catalysts posses both the Lewis acidic sites as well as Brønsted acidic sites which both can catalyze the esterification reaction [55, 56]. In the Lewis acidic sites catalyzed esterification reaction (Path I), the adsorption of carbonyl group of the carboxylic acid in LA on the Lewis acidic site takes place increasing the electrophilicity at the carbonyl carbon. The Lewis acidity originates from the O=W=O of the tungsten oxide incorporated SBA-16 [44, 47]. The nucleophilic attack of the oxygen atom of the alcohol on the carbonyl carbon followed by the dehydration leads to the formation of levulinate ester. In the Brønsted acidic sites catalyzed esterification reaction (Path II), the adsorption of carbonyl group of the carboxylic acid of the LA on the Brønsted acidic sites which are originate from W- OH of the tungsten oxide incorporated SBA-16 leads to the generation of electrophilic carbonyl carbon [44, 47, 55]. The subsequent nucleophilic attack followed by dehydration step forms the levulinate ester. In the present case, the most of the levulinate ester is produced by path I as the number of Lewis acidic sites are dominant compared to Brønsted acidic sites. The

formation of angelica lactones takes place by either Lewis acidic sites or Brønsted acidic sites [57, 58]. The adsorption of carbonyl group (keto) of LA instead of carbonyl group of carboxylic acid in LA on Lewis acidic site or Brønsted acidic site creates an electrophilic centre at the carbonyl carbon (keto). The intra molecular nucleophilic attack of the oxygen atom of the carboxylic acid group in LA and subsequent dehydration leads to the formation of angelica lactones.

3.2.2. Effect of molar ratio

The effect of molar ratio of LA to ethanol on the selectivity to EL was studied over 3WS catalyst and results were depicted in Figure 10. The LA to ethanol molar ratio varied from 1:1 to 1:11. The selectivity towards EL increases with increase in molar ratio of LA to ethanol from 1:1 to 1:7 and reaches a maximum selectivity of 95% at a molar ratio of 1:7. Further increase in the concentration of ethanol results gradual decrease in selectivity to EL from 95% to 87% (at molar ratio of 1:11). These results can be ascribed as the esterification reaction of LA with ethanol is a reversible reaction, high amount of alcohol is necessary to favor the forward reaction. However, an excess amount of alcohol may dilute the reactant there by decreasing the selectivity to the EL due to mass transfer limitation. Hence, it can be suggested that maximum selectivity to EL can be achieved in this reaction with an optimum molar ratio of 1:7 (LA: ethanol).

3.2.3. Effect of temperature

The effect of temperature ranging from 250 °C (near to the boiling point of LA [27]) to 310 °C on the esterification of LA with ethanol was studied on 3WS catalyst and the results were depicted in Figure 11. At all the temperatures the conversion of LA is found to be complete, with a variation in the selectivity to EL. As the temperature increases from 250 °C to 310 °C, the

selectivity to EL decreases due to the formation of angelica lactones through dehydration of LA. These results suggest that the favorable temperature for this esterification of LA is 250 °C.

3.2.4. Influence of Time on stream

A time on stream study was conducted over 3WS catalyst under optimized reaction conditions and the results were illustrated in Figure 12. The results indicate stable catalytic activity of the 3WS catalyst during 10 h time on stream study. The conversion of LA is constant during the time of study, while the selectivity to EL decreases slightly. For the sake of comparison, a WO_3/SBA-16 catalyst with 3 weight % WO_3 prepared by impregnation method (3WS-I) has been subjected for the time on stream study for the levulinc acid esterification with ethanol and the results are shown in Figure 13. This catalyst experiences a loss in the conversion of levulinic acid from 91 % (initial conversion) to 72 % at the end of 10^{th} hour. Continuous decrease in the selectivity towards ester (EL) has been observed over this catalyst. Thus 3WS maintains steady activity compared to the catalyst with same WO_3 loading prepared by impregnation method. Interestingly, the spent 3WS catalyst was regenerated by performing calcination in flow of air after completion of each cycle. The regenerated catalysts exhibit similar catalytic activity in the esterification reaction of LA with ethanol during 10 h time on stream of 10 cycles (Figure 12). The 3WS could be regenerated for 10 cycles. The conversion of LA is consistent while the selectivity to EL is slightly decreased from 88% to (initial selectivity at first hour) to 77 % (10^{th} hour) at the end of the 10^{th} cycle. The slight decrease in the catalytic activity of the catalyst may be due to the poisoning of catalyst surface by water molecules released during the esterification reaction or due to the deposition of carbonaceous species over the catalyst surface. The poisoning of catalyst surface by water molecules is obvious in the case of catalysts containing conventional supports like hydrotalcites, magnesia etc. The hydrophobic

nature of the mesoporous silica helps to maintain the catalytic activity in water released catalytic reactions [59]. In the present study, tungsten oxide incorporated mesoporous silica (SBA-16) resists the water molecules to adsorb on the catalyst surface. Hence, there is no scope for the poisoning of catalyst surface by water molecules released during the reaction. The spent catalyst was characterized to know the reason for the slight decline in the catalytic activity of the 3WS catalyst in the esterification reaction. It could be observed that there is no change in the small angle and wide angle XRD patterns of the catalysts (results were not shown), indicating the retention of mesoporous 3D structure of 3WS catalyst. The total acidity of the fresh 3WS catalyst (0. 23 mmol NH_3 g^{-1}) decreases to (0.15 mmol NH_3 g^{-1}) after 10^{th} cycle (10^{th} hour) and it regains to similar extent (0.19 mmol NH_3 g^{-1}) after calcination in flow of air. The decrease in acidity of the 3WS catalyst after the reaction is due to the deposition of carbonaceous species over the catalyst surface. The regaining acidity of the regenerated catalyst is due to the removal of carbonaceous species during the calcination in flow of air. Further, CHNS analysis shows the presence of carbon in the spent catalyst, supporting the deposition of carbonaceous species. From these investigations, the slight decrease in the catalytic activity is due to the deposition of carbonaceous species over the catalyst surface.

3.2.5. Influence of different alcohols

The catalytic performance of the 3WS catalyst in the esterfication of LA with different alcohols was tested to know the efficiency of the catalyst and the results were illustrated in Figure 14. The 3WS catalyst shows superior catalytic performance in the selective synthesis of alkyl levulinates from LA with methanol (MeOH), ethanol (EtOH), n-propanol (PrOH), and n-butanol (BuOH). The complete conversion of LA is observed with corresponding yields of the alkyl levulinates are 96, 95, 94 and 94 % respectively. A decrease in the conversion of LA (93

and 64 %) and yields of the alkyl levulinates (61 and 13 %) are noticed with isopropanol (2-PrOH) and isobutanol (2-BuOH) respectively. The drop in activity with secondary alcohols may be due to steric hindrance on hydroxyl group of the alcohol, which reduces the nucleophilic attack of the hydroxyl group of alcohol on carbonyl carbon of the carboxylic acid group in LA.

4. Conclusions

In conclusion, tungsten oxide incorporated SBA-16 catalysts were successfully synthesized in one pot direct synthesis method and applied to the esterification of LA with alcohols in continuous process at atmospheric pressure. X-ray diffraction, N_2 physisorption suggest the retention of 3D mesoporous structure in the tungsten incorporated SBA-16 catalysts. SEM and TEM techniques show the morphological aspects in the investigated catalysts. DR-UV-vis spectroscopy, temperature programmed reduction, EDX analysis show the presence of tungsten in the synthesized catalysts. The temperature programmed desorption of ammonia demonstrated the acidity of the catalysts. Under optimized reaction conditions, 3WS catalyst exhibits highest selectivity (95%) to EL with complete conversion of LA. The superior catalytic performance of the catalyst can be assigned to the enhanced acidity of SBA-16 due to the incorporation of tungsten oxide, possessing well dispersed accessible acidic sites through uniform pore channels. The 3WS catalyst shows stable catalytic activity during the 10 hours time on stream study for 10 cycles. The slight decline in the selectivity to EL is due to the deposition of carbonaceous species over the catalyst surface. The selective formation of alkyl levulinates (methyl, ethyl, n-propyl, and n-butyl, more than 90%) designates the excellence of the 3WS catalyst in the esterification of LA with alcohols in continuous process.

Acknowledgements

The authors E.S.S, G.V.R.B and C.R.R gratefully thank University Grant Commission, New Delhi, for financial support.

References

[1] J. V. Veer, The Times (2007), June 25.

[2] J. Khler, L. Whitmarsh, B. Nysvist, M. Schilperoord, N. Bergman, A. Haxeltine, Ecological Economics, 68 (2009) 2985–2995.

[3] B. E. Dale, S. Kim in Biorefineries: Industrial Processes and Products, Vol. 1 (Eds.: B. Kamm, P. R. Gruber, M. Kamm), Wiley-VCH, Weinheim, (2006) 41–66.

[4] X. Yan, O. R. Inderwildi, D. A. King, Energy Environ. Sci., 3 (2010) 190–197.

[5] P. Maki-Arvela, B. Holmbom, T. Salmi, D. Murzin, Catal. Rev. Sci. Eng., 49 (2007) 197– 340.

[6] M. J. Climent, A. Corma, S. Iborra, Green Chem., 16 (2014) 516–547.

[7] H. Kobayashi, A. Fukuoka, Green Chem., 15 (2013) 1740−1763.

[8] M. J. Climent, A. Corma, S. Iborra, Green Chem., 13 (2011) 520−540.

[9] K. Yan, C. Jarvis, J. Gu, Y. Yan, Renewable and Sustainable Energy Reviews, 51 (2015) 986-997.

[10] E. S. Sankar, G. V. Ramesh Babu, K. Murali, B. David Raju, K. S. Rama Rao, RSC Adv., 6 (2016) 20230-20239.

[11] A. Démolis, N. Essayem, F. Rataboul, ACS Sustainable Chem. Eng., 2 (2014) 1338−1352.

[12] H. Joshi, B. R. Moser, J. Toler, W. F. Smith, T. Walker, Biomass Bioenerg., 35 (2011) 3262–3266.

[13] E. Christensen, A. Williams, S. Paul, S. Burton, R. L. McCormick, Energy Fuels, 25 (2011) 5422–5428.

[14] F. Su, Q. Wu, D. Song, X. Zhang, M. Wanga, Y. Guo, J. Mater. Chem. A, 1 (2013) 13209–13221.

[15] G. Pasquale, P. Vázquez, G. Romanelli, G. Baronetti, Catal. Commun., 18 (2012) 115–120.

[16] D. R. Fernandes, A. S. Rocha, E.F. Mai, Claudio J. A. Mota, V. Teixeira da Silva, Appl. Catal. A Gen., 425–426 (2012) 199–204.

[17] C. R. Patil, P. S. Niphadkar, V. V. Bokade, P. N. Joshi, Catal. Commun., 43 (2014) 188-191.

[18] C. M. Kalpana, J. Kozinski, A. Dalai, Catal. Lett., 143 (2013) 1220–1225.

[19] R. D. Wilson, D. G. Barton, C. D. Baertsch, E. Iglesia, J. Catal., 194 (2000) 175-187.

[20] J. Ramirez, A. G. Alejandre, J. Catal., 170 (1997)108-122.

[21] Y. Sakamoto, M. Kaneda, O. Terasaki, D. Y. Zhao, J. M. Kim, G. Stucky, H. J. Shin, R. Ryoo, Nature, 408 (2000) 449-453.

[22] L. Zhang, W. Zhu, Q. Lin, J. Han, L. Jiang, Y. Zhang, International Journal of Nano medicine, 10 (2015) 3291–3302.

[23] Y. Hao, Y. Chong, S. Li, H. Yang, J. Phys. Chem. C, 116 (2012) 6512−6519.

[24] V. Mohan, V. Venkateshwarlu, G. Saidulu, B. David Raju, K. S. Rama Rao, RSC Adv., 5 (2015) 57201–57210.

[25] A. T. Shah, B. Li, Z. E. A. Abdalla, Microporous Mesoporous Mater., 130 (2010) 248-254.

[26] M. Rajamanickam, M. P. Pachamuthu, A. Ramanathan, B. Subramaniam, Ind. Eng. Chem. Res., 53 (2014) 18833–18839.

[27] E. Siva Sankar, V. Mohan, M. Suresh, G. Saidulu, B. David Raju, K. S. Rama Rao Catal. Commun., 75 (2016) 1-5.

[28] F. Kleitz, T. W. Kim, R. Ryoo, Langmuir, 22 (2005) 440-445.

[29] W. J. J. Stevens, K. Lebeau, M. Mertens, G. V. Tendeloo, P. Cool, E. F. Vansant, J. Phys. Chem. B, 110 (2006) 9183-9187.

[30] J. Cheng Hu, Y. D. Wang, Li. F. Chen, R. Richards, W. M. Yang, Z. Cheng Liu, W. Xu, Microporous Mesoporous Mater., 93 (2006) 158–163.

[31] X. L. Yang, W. L. Dai, H. Chen, J. H. Xu, Y. Cao, H. X. Li, K. N. Fan, Appl. Catal. A: Gen., 283 (2005) 1-8.

[32] H. Liu, K. Tao, P. Zhang, W. Xua, S. Zhou, New J. Chem., 39 (2015) 7971- 7978.

[33] P. I. Ravikovitch , A. V. Neimark, Langmuir, 18 (2002)1550-1560.

[34] A. Ramanathan, M. Rajamanickam, B. P. Grady, D.S. Moore, D. H. Barich, B. Subramaniam, Microporous Mesoporous Mater., 175 (2013) 43–49.

[35] K. Miyasaka, H. Hano, Y. Kubota, Y. Lin, R. Ryoo, M. Takata, S. Kitagawa, A. V. Neimark, O. A. Terasaki, Chem. Eur. J., 18 (2012) 10300-10311.

[36] W. J. J. Stevens , M. Mertens , S. Mullens , I. Thijs , G. V. Tendeloo , P. Cool , E. F. Vansant, Microporous Mesoporous Mater., 93 (2006) 119–124.

[37] A. B. Mohamed, J. M. Córdoba, M. Odén, Microporous Mesoporous Mater., 129 (2010) 106–111.

[38] O. C. Gobin, Y. Wan, D. Zhao, F. Kleitz, S. Kaliaguine, J. Phys. Chem. C, 111 (2007) 3053-3058.

[39] Y. K. Hwang, J. S. Chang, Y. U. Kwon, S. E. Park, Microporous Mesoporous Mater., 68 (2004) 21–27.

[40] A. Tuel, S. Gontier, R. Teissier, Chem. Commun., (1996) 651-652.

[41] T. Blasco, A. Corma, M. T. Navarro, J. Perez-Pariente, J. Catal., 156 (1995) 65-74.

[42] J. S. Reddy, A. Sayari, J. Chem. Soc., Chem. Commun., (1995) 2231-2232.

[43] A. Bordoloi, A. Vinub, S. B. Halligudi, Chem. Commun., 2007, 4806–4808.

[44] B. Hu, H. Liu, K. Tao, C. Xiong, S. Zhou, J. Phys. Chem. C, 117 (2013) 26385−26395.

[45] Y. Shao, L. Wang, J. Zhang, M. Anpo, J. Phys. Chem. B, 109 (2005) 20835-20841.

[46] B. L. Newalkar, J. Olanrewaju, S. Komarneni, Chem. Mater., 13 (2001) 552-557.

[47] Xin-Li Yang, Wei-Lin Dai, Ruihua Gao, Kangnian Fan, J. Catal., 249 (2007) 278–288

[48] D. C. Vermaire, P. C. Vanberge, J. Catal., 116 (1989) 309-317.

[49] L. Karakonstantis, H. Matralis, Ch. Kordulis, A. Lycourghiotis, J. Catal., 162 (1996) 306-319.

[50] J. A. Horsley, I. E. Wachs, J. M. Brown, G. H. Via, F. D. Hardcastle, J. Phys. Chem., 91 (1987) 4014-4020.

[51] V. Mohan, V. Venkateshwarlu, C. V. Pramod, B. D. Raju, K. S. Rama Rao, Catal. Sci. Technol., 4 (2014)1253-1259.

[52] A. Ramanathan, B. Subramaniam, D. Badloe, U. Hanefeld, R. Maheswari, J. Porous Mater., 19 (2012) 961–968.

[53] T. I. Bhuiyan, P. Arudra, M. N. Akhtar, A. M. Aitani, R. H. Abudawoud, M. A. Al-Yami , S. S. Al-Khattaf, Appl. Catal. A: Gen., 467 (2013) 224–234.

[54] C. Martin, P. Malet, G. Solana, V. Rives, J. Phys. Chem. B, 102 (1998) 2759-2768.

[55] A. S. Khder, E. A. El-Sharkawy, S. A. El-Hakam, A. I. Ahmed, Catal. Commun., 9 (2008) 769–777.

[56] F. Su, Q. Wu, D. Song, X. Zhang, M. Wanga , Y. Guo, J. Mater. Chem. A, 1 (2013) 13209-13221.

[57] V. V. Kumar, G. Naresh, M. Sudhakar, J. Tardio, S. K. Bhargava, A. Venugopal, Appl. Catal. A: Gen., 505 (2015) 217-223.

[58] V. Mohan, C. Raghavendra, C. V. Pramod, B. D. Raju, K. S. R. Rao, RSC Adv., 4 (2014) 9660-9668.

[59] V. Mohan, C.V. Pramod, M. Suresh, K. H. P. Reddy, B. D. Raju, K.S. R. Rao, Catal. Commun., 18 (2012) 89–92.

Figure captions

Figure 1 Low angle XRD patterns of pristine SBA-16 and WO_3- SBA-16 samples and in inset figure wide angle XRD patterns of WO_3- SBA-16 samples

Figure 2 N_2 adsorption-desorption isotherms for pristine SBA-16 and WO_3- SBA-16 samples and in inset figure pore size distribution of pristine SBA-16 and WO_3- SBA-16 samples

Figure 3 SEM images of (a) pristine SBA-16 (b) 3WS (c) EDX spectrum of 3WS, TEM images of (c) pristine SBA-16 and (d) 3WS

Figure 4 UV-Vis-DRS spectra of WO_3 and WO_3- SBA-16 samples

Figure 5 FT-IR spectra of SBA-16 and WO_3- SBA-16 samples

Figure 6 H_2-TPR patterns of WO_3 and WO_3- SBA-16 samples

Figure 7 TPD profiles of SBA-16 and WO_3- SBA-16 samples

Figure 8 Pyridine adsorbed FT-IR spectra of SBA-16 and WO_3- SBA-16 samples

Figure 9 Effect of WO_3 loading on esterification of LA with EtOH
Reaction conditions: Catalyst weight: 0.5 g, LA: EtOH =1:7 reaction temperature: 250 ºC, N_2 flow: 30 mL min^{-1}, Liquid feed flow: 1 mL h^{-1}

Figure 10 Effect of molar ratio of LA to EtOH on esterification of LA with EtOH
Reaction conditions: Catalyst weight: 0.5 g, reaction temperature: 250 ºC, N_2 flow: 30 mL min^{-1}, Liquid feed flow: 1 mL h^{-1}

Figure 11 Effect of reaction temperature on esterification of LA with EtOH
Reaction conditions: Catalyst weight: 0.5 g, LA: EtOH =1:7, N_2 flow: 30 mL min^{-1}, Liquid feed flow: 1 mL h^{-1}

Figure 12 Influence of time on stream esterification of LA with EtOH

Reaction conditions: Catalyst weight: 0.5 g, LA: EtOH =1:7 reaction temperature: 250 ºC, N_2 flow: 30 mL min^{-1}, Liquid feed flow: 1 mL h^{-1}

Figure 13 Influence of time on stream on esterification of LA with EtOH over 3WS-I catalyst. Reaction conditions: Catalyst weight: 0.5 g, LA: EtOH =1:7 reaction temperature: 250 ºC, N_2 flow: 30 mL min^{-1}, Liquid feed flow: 1 mL h^{-1}

Figure 14 Influence of various alcohols on esterification of LA

Reaction conditions: Catalyst weight: 0.5 g, LA: Alcohol =1:7 reaction temperature: 250 ºC, N_2 flow: 30 mL min^{-1}, Liquid feed flow: 1 mL h^{-1}

Scheme 1 Plausible reaction pathway for the esterification of levulinic acid with alcohols over WO_3-SBA-16 catalyst

Scheme 2 Plausible reaction pathway for the formation of angelica lactones over WO_3-SBA-16 catalyst

Figure 1

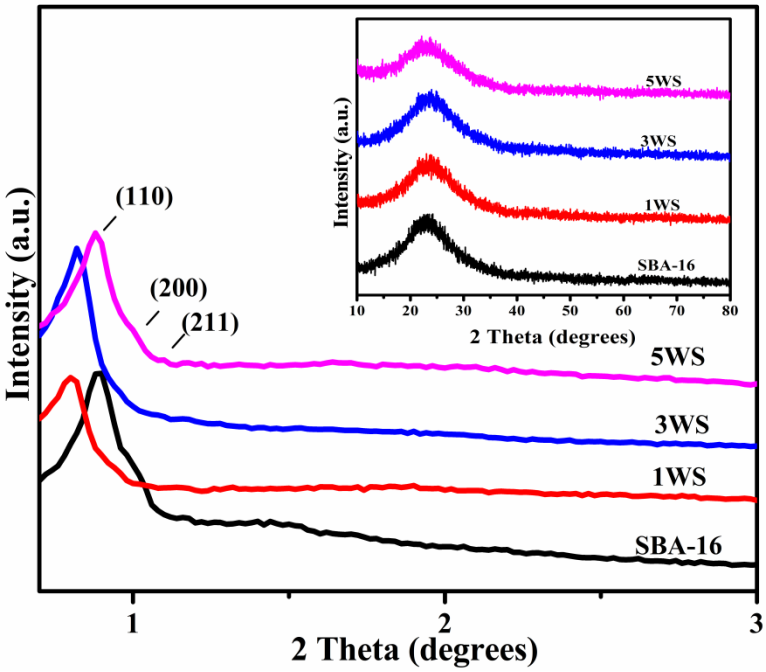

Figure 2

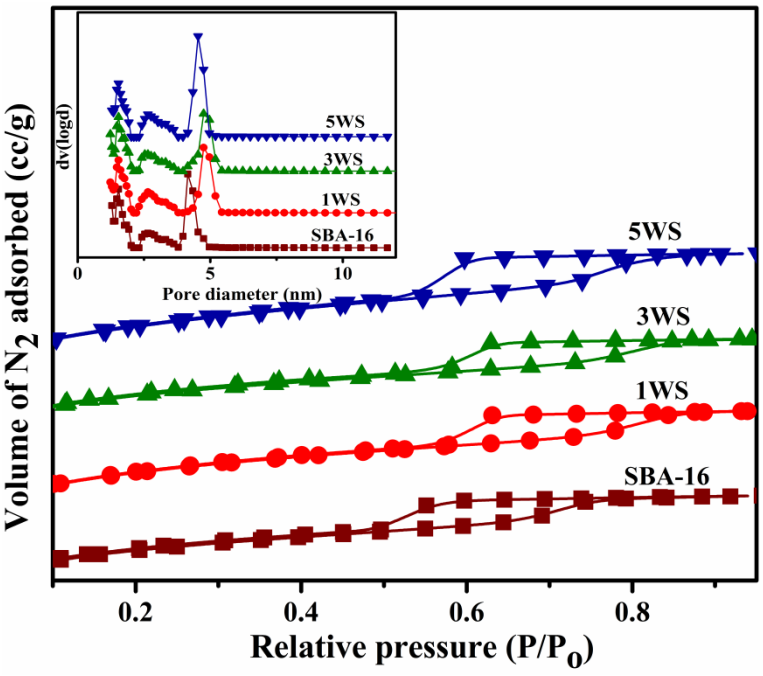

Figure 3

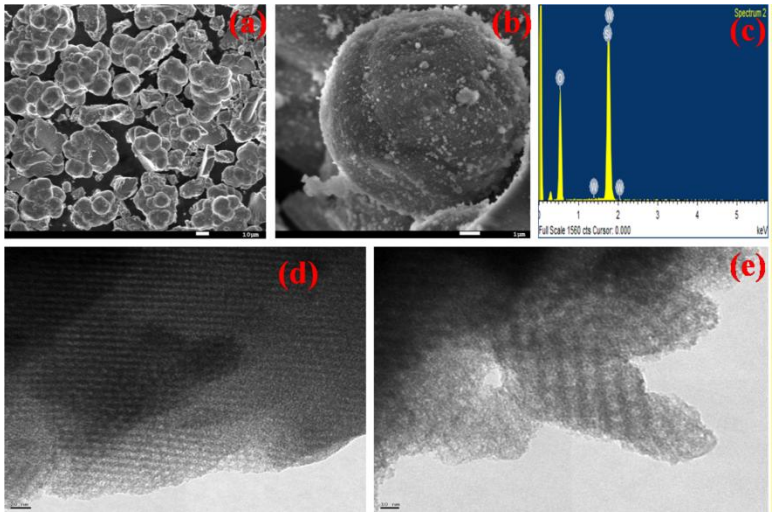

Figure 4

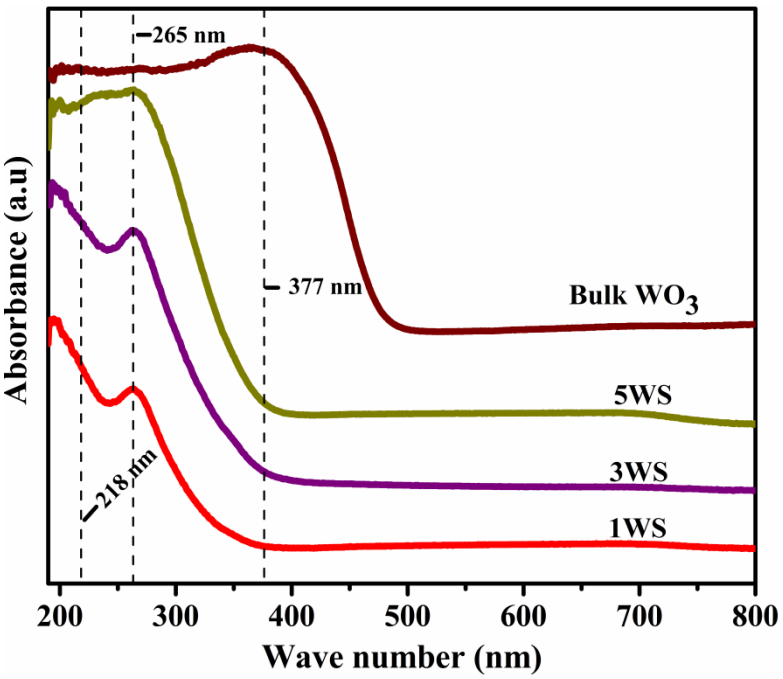

Figure 5

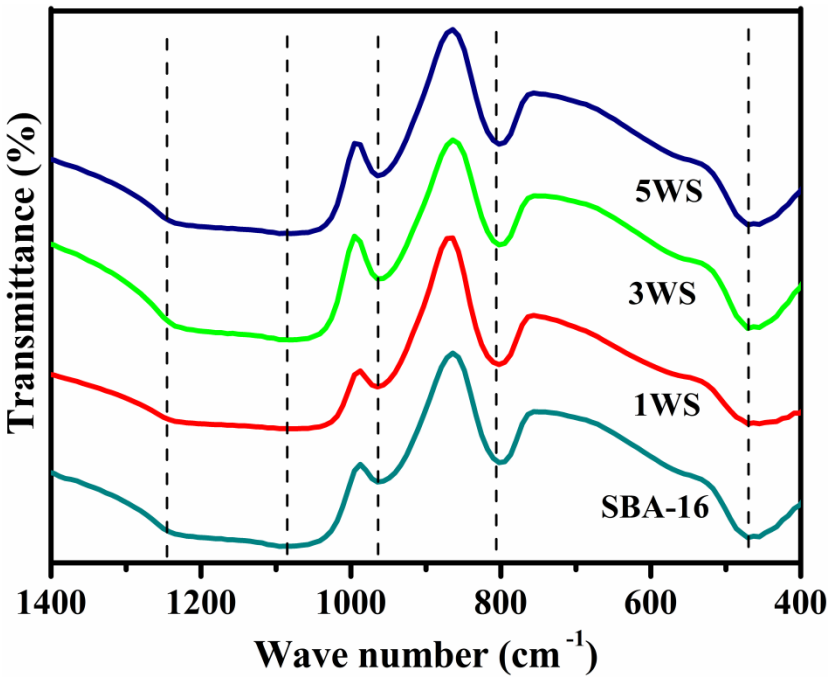

Figure 6

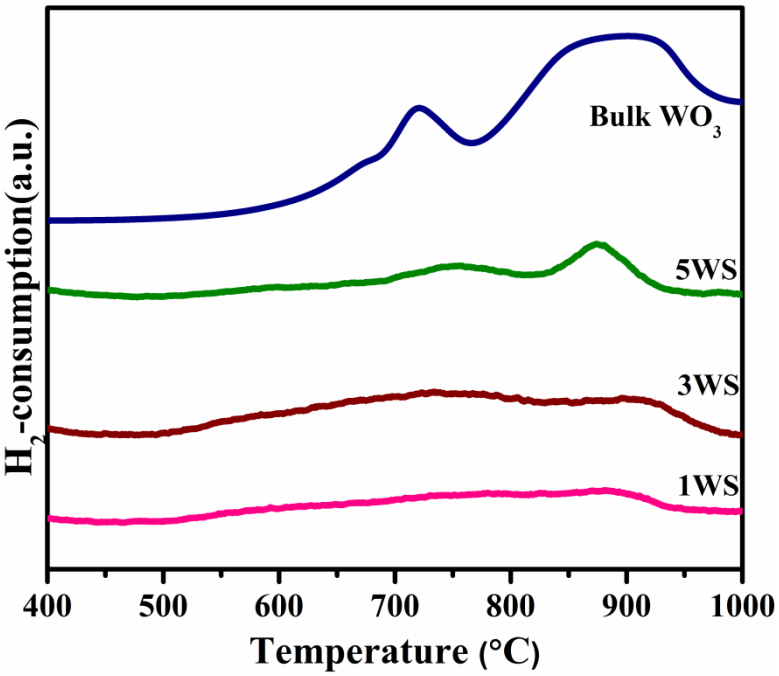

Figure 7

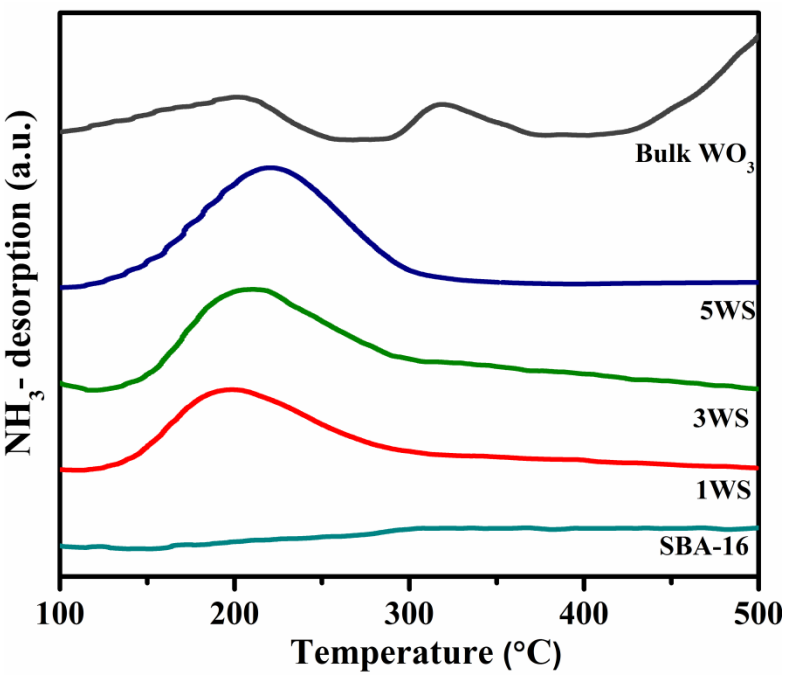

Figure 8

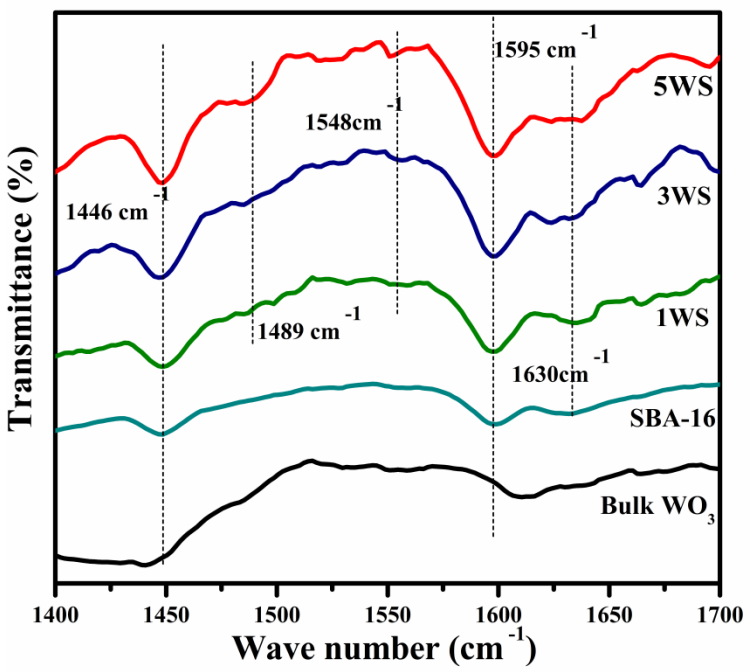

Figure 9

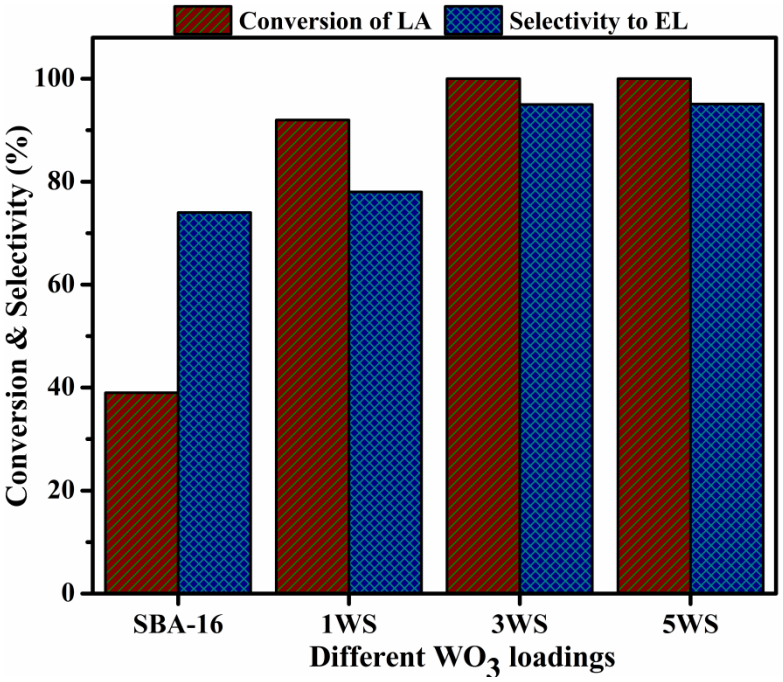

Figure 10

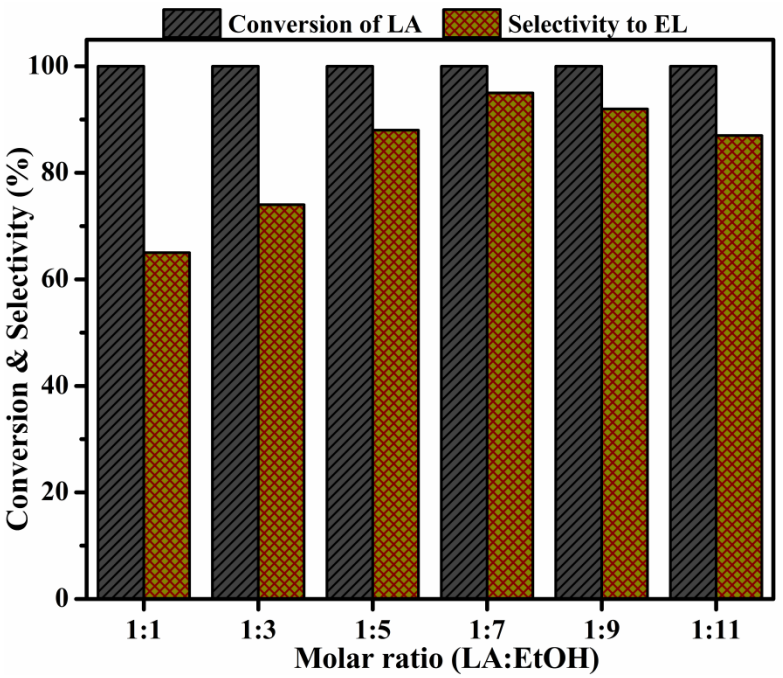

Figure 11

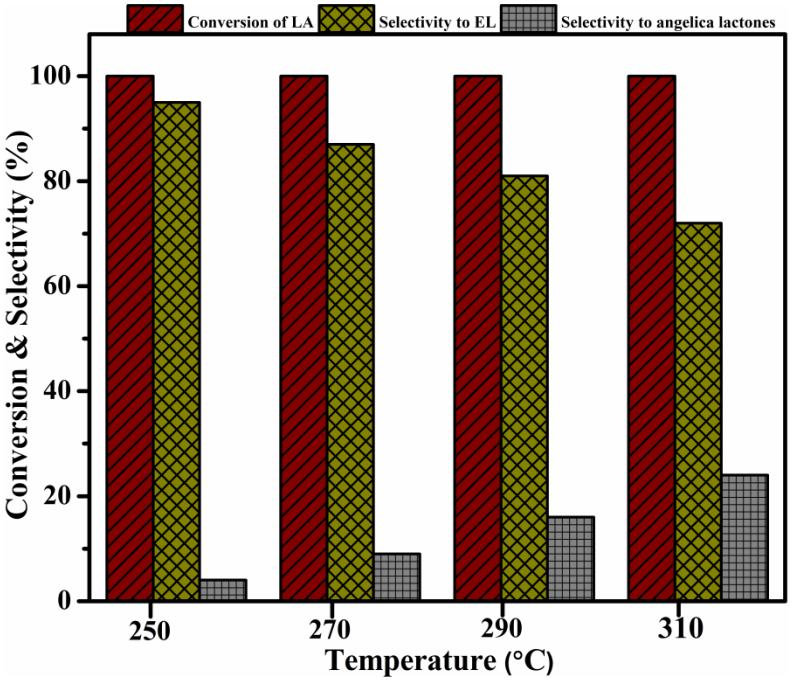

Figure 12

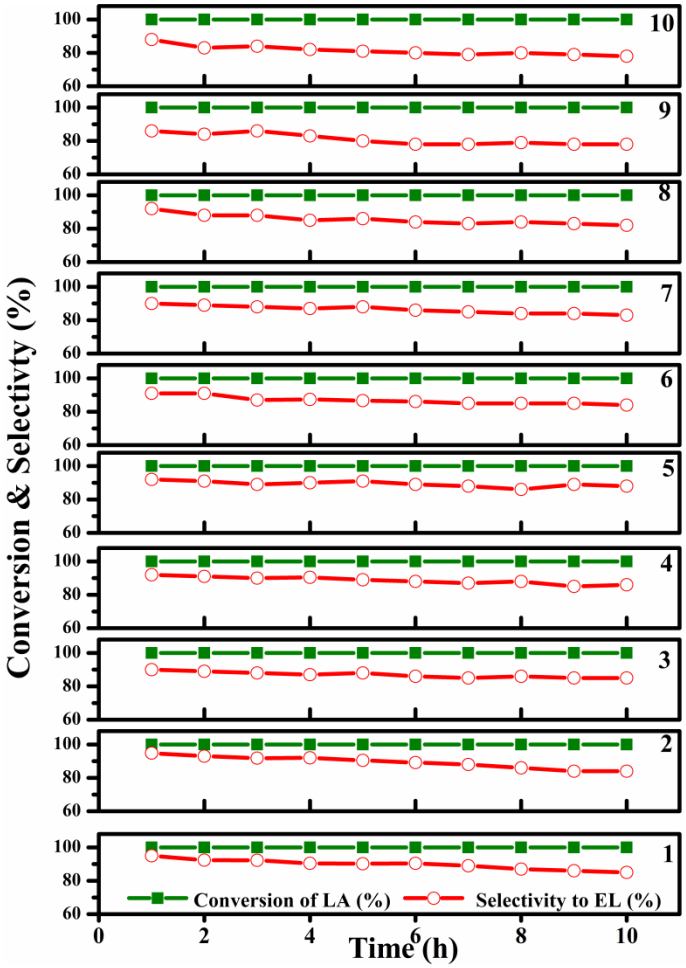

Figure 13

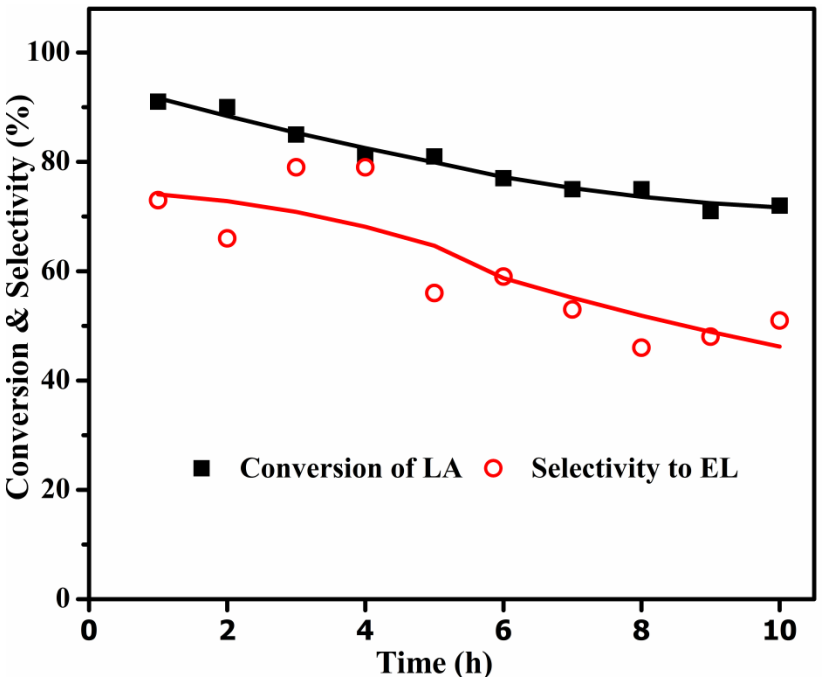

Figure 14

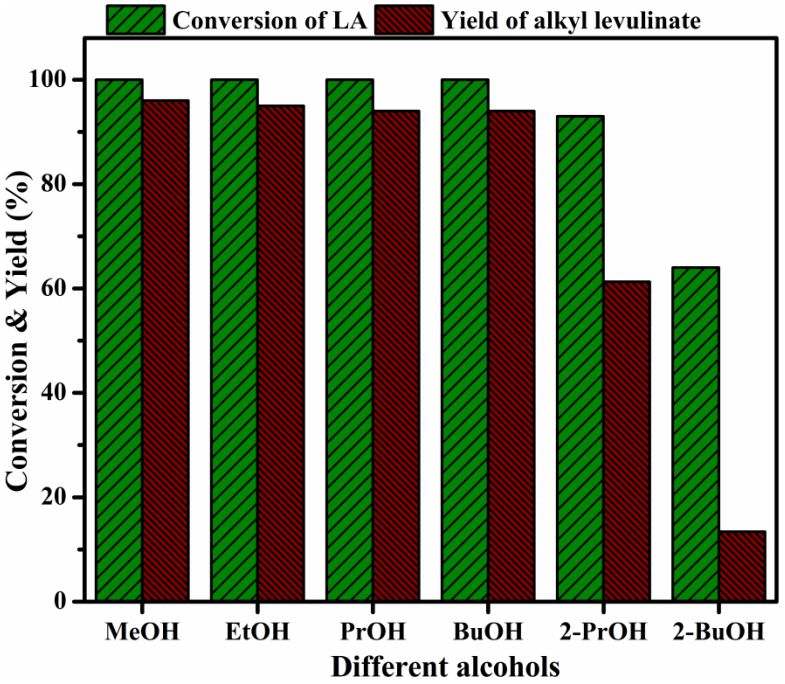

Scheme-1

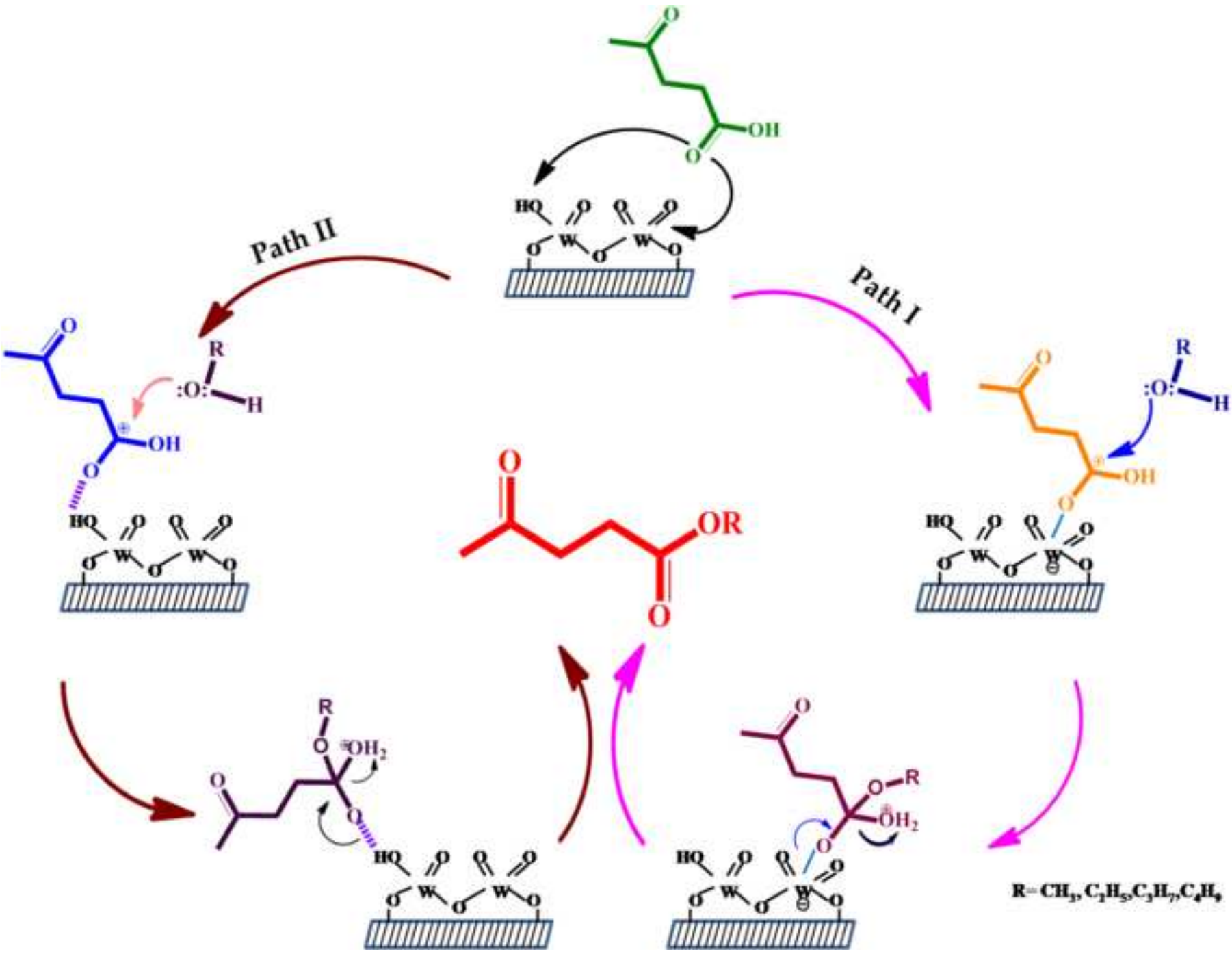

Scheme-2

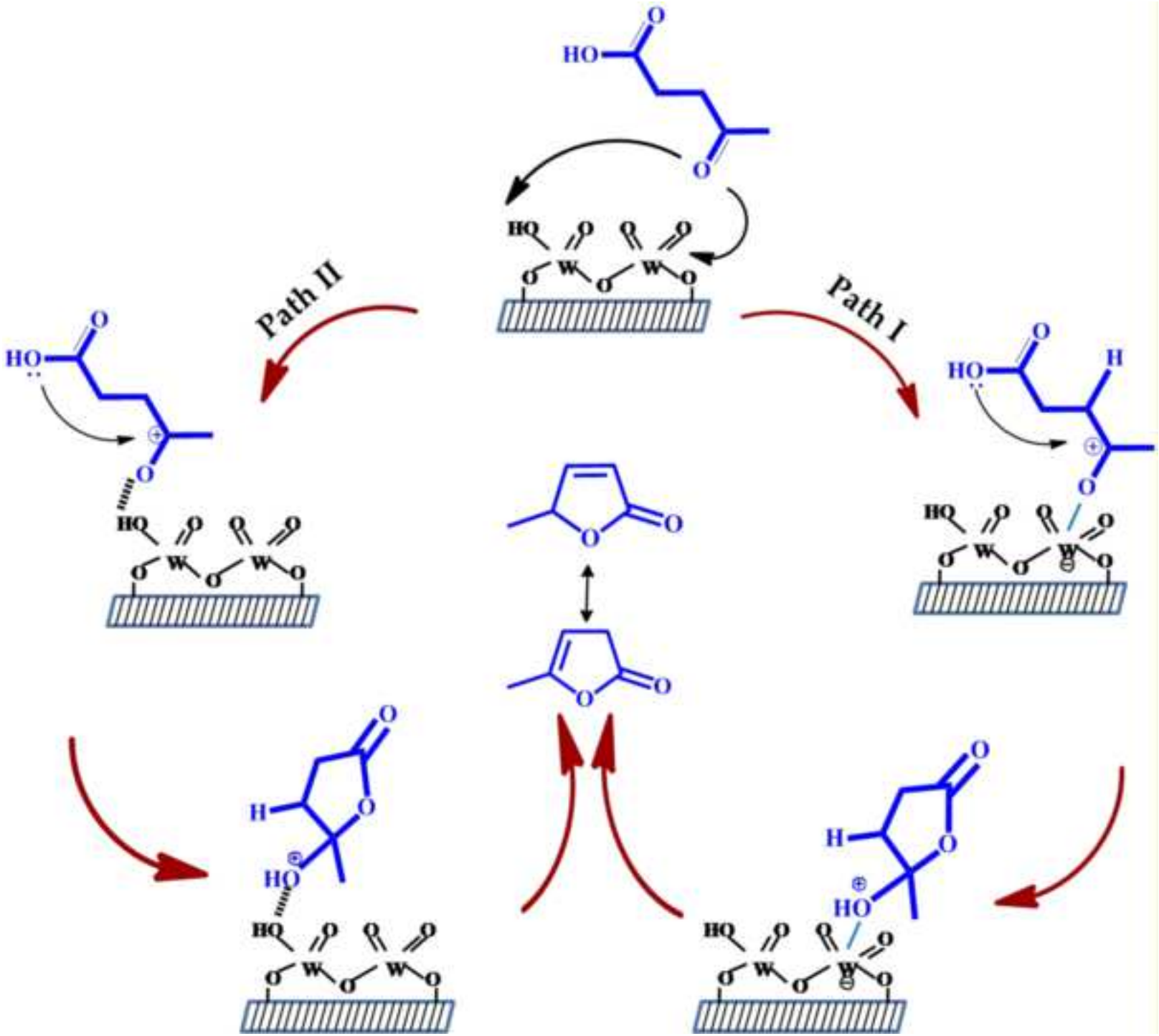

Table 1 Textural and structural parameters of SBA-16 and WO_3-SBA-16 catalysts

Catalyst	S_{BET}[a] ($m^2 g^{-1}$)	S[b] ($m^2 g^{-1}$)	V_t[c] (cc/g)	D[d] (nm)	d $_{(110)}$ [e] (nm)	a_o[f] (nm)	t[g] (nm)
SBA-16	762	762	0.95	4.15	9.01	12.74	6.88
1WS	734	741	0.99	4.75	10.98	15.52	8.69
3WS	725	747	0.98	4.76	10.74	15.18	8.38
5WS	710	747	0. 95	4.54	10.10	14.28	7.82
WO_3	16	-	0.02	3.18	-	-	-

[a] BET Surface area [b] Surface area per gram of support [c] Total Pore Volume [d] Average Pore size [e] Periodicity of SBA-16 derived from a low angle XRD. [f] Unit cell parameter = $2^{½}$ $d_{(110)}$ [g] Pore wall thickness = $(3^{½}a_0/2)$- D

Table 2 WO_3 loading and acidity of WO_3-SBA-16 catalysts

Catalyst	Theoretical WO_3 Loading (Wt %)	WO_3 loading by EDX (Wt %)	Acidity ($mmolNH_3/g$)
SBA-16	0	0	0.01
1WS	1	0.8	0.14
3WS	3	2.7	0.23
5WS	5	4.3	0.29
WO_3	-	-	0.18